Interatomic potential for the Al-Cu system

F. Apostol[*] and Y. Mishin[†]

Department of Physics and Astronomy, MSN 3F3, George Mason University, Fairfax, Virginia 22030, USA

(Received 10 November 2010; revised manuscript received 20 January 2011; published 25 February 2011)

An angular-dependent interatomic potential has been developed for the Al-Cu system based on existing embedded-atom method potentials for Al and Cu and fitting of the cross-interaction functions to experimental and first-principles data. The potential reproduces lattice parameters, formation energies, and elastic constants of the θ and θ' phases of this system. It predicts the θ' phase to be more stable than θ at 0 K but to become less stable at hight temperatures due to vibrational entropy. The temperate and entropy of this phase transformation are in good agreement with previous first-principles calculations [C. Wolverton and V. Ozoliņš, Phys. Rev. Lett. **86**, 5518 (2001)]. The potential provides a reasonable description of the phase stability across the Al-Cu phase diagram, dilute heats of solution, and other thermodynamic properties. It has also been tested for generalized stacking fault energies in the presence of a copper layer embedded in Al. This configuration bears some resemblance to Guinier-Preston zones that strengthen Al-Cu alloys. The trends predicted by the potential for uniform shearing of this configuration are in agreement with results of first-principles density-functional calculations performed in this work. The potential is expected to be suitable for atomistic simulations of precipitation hardening of Al-Cu alloys.

I. INTRODUCTION

Al-Cu–based alloys are widely used in aircraft structures due to their low density and much higher mechanical strength in comparison with pure Al. The strength of Al-Cu alloys is due to an effect called precipitation hardening. During isothermal aging of a Al(Cu) solid solution supersaturated with Cu, uniformly dispersed Cu-rich precipitates (particles) are formed by diffusion of Cu. These precipitates create obstacles to dislocation glide during plastic deformation of the alloy. The dislocations are forced either to cut through the precipitates or to loop around them, increasing the strength of the alloy.

The well-established precipitation sequence during the aging process consists of several steps: solid solution → Guinier-Preston (GP) zones → θ'' particles (GP II zones) → θ' phase particles → θ phase particles.[1] GP zones, independently discovered in 1938 by Guinier[2] and Preston,[3] are disk-shaped monolayers of Cu aligned along {100} planes of the fcc Al lattice. The θ'' particles are clusters of two or more {100} Cu layers separated by three aluminum planes. The θ' particles are larger, are semicoherent with the Al matrix, and contain a metastable Al_2Cu phase with a tetragonally distorted calcium fluorite structure. Finally, the θ particles are even larger, are incoherent with the matrix, and have the same Al_2Cu stoichiometry as θ' but a tetragonal C16 structure. The θ phase is the thermodynamically stable phase that appears in the phase diagram of the Al-Cu system at elevated temperatures.[1]

Wolverton and Ozoliņš[4] have shown by first-principles calculations that at 0 K, the θ' phase has a lower energy than θ. According to their calculations, it is the vibrational entropy that stabilizes θ over θ' at temperatures higher than about 473 K. In alloy processing technology, it is desirable to avoid the $\theta' \rightarrow \theta$ transformation during the aging anneal because it significantly lowers the mechanical strength of the alloy (the "overaging" effect). It is the GP zones and the θ' phase that are most important for the precipitation hardening effect, whereas the θ phase is less important.

Significant insights into the strengthening mechanisms can be obtained by large-scale molecular dynamics simulations; see, for example, the recent study of the strengthening by GP zones.[5] To afford large ensembles of atoms and long simulation times, such simulations use semiempirical interatomic potentials.[6] While such potentials cannot be as accurate as first-principles calculations, they are computationally fast and can capture some of the key features of the strengthening effect. The goal of this work is to develop an accurate (within intrinsic limitations of the semiempirical approach) potential for the Al-Cu system that could be suitable for atomistic simulations of precipitation and hardening in Al-Cu alloys.

Several Al-Cu potentials can be found in the literature. Cai and Ye[7] developed a set of embedded-atom method (EAM) potentials for seven fcc metals and their binary alloys, including Al-Cu. For the cross-pair potential function, which defines properties of the binary system, they used a density-weighted combination of the monoatomic pair potentials[8] without any fitting parameters. The dilute heat of solution, ΔE_s, of Cu in Al was reported to be −1.29 eV,[7] which is almost an order of magnitude larger than the experimental value of −0.142 eV.[9] Properties of the θ and θ' phases were not tested with this potential and the formation energies of the $L1_2$ (Al_3Cu and $AlCu_3$) and $L1_0$ (AlCu) structures are not in close agreement with first-principles results.[10,11] The EAM potential of Rohrer,[12] designed for Al-Cu-Ag solid solutions, predicts accurate values of ΔE_s for Al in Cu and of the Cu-vacancy binding energy in Al. But this potential underestimates the ΔE_s of Cu in Al as −0.041 eV. The potential was not tested for properties of Al-Cu compounds. The EAM potential of Liu *et al.*[13] was obtained by fitting the lattice parameters and formation energy of the θ phase as well as the dilute heats of solution and some other properties of the Al-Cu system. As shown later, this potential does not reproduce the correct stability of the θ' phase. The recent modified embedded-atom method (MEAM) potential of Hu *et al.*[14] correctly predicts the θ' phase to be more stable than θ at 0 K. This potential reproduces the crossing of the θ and θ' free energies at 260 K.

Hu *et al.*[14] do not report on elastic properties of the θ and θ' phases, the phase stability across the Al-Cu phase diagram, or other properties of the Al-Cu system.

In this work we propose an interatomic potential for the Al-Cu system based on the angular-dependent potential (ADP) formalism,[15–18] which is a generalization of the traditional EAM method[19,20] to include angular-dependent interactions. The potential development methodology is described in Sec. II. The testing procedures and results are presented in Secs. III and IV, followed by conclusions in Sec. V. We use the potential of Liu *et al.*[13] (which is referred to as the LLB potential) for comparison with our potential throughout the paper.

II. POTENTIAL DEVELOPMENT

In the ADP method,[15–18] the total energy E_{tot} of a collection of atoms is represented in the form

$$E_{\text{tot}} = \frac{1}{2} \sum_{i,j(j \neq i)} \Phi_{s_i s_j}(r_{ij}) + \sum_i F_{s_i}(\bar{\rho}_i) + \frac{1}{2} \sum_{i,\alpha} \left(\mu_i^\alpha\right)^2$$
$$+ \frac{1}{2} \sum_{i,\alpha,\beta} \left(\lambda_i^{\alpha\beta}\right)^2 - \frac{1}{6} \sum_i \nu_i^2, \quad (1)$$

where indices i and j refer to atoms and superscripts α, $\beta = 1$, 2, 3 to Cartesian directions. $\Phi_{s_i s_j}(r_{ij})$ is the pair-interaction potential, which depends only on the scalar distance r_{ij} between atom i and atom j and on their chemical species s_i and s_j. The function $F_{s_i}(\bar{\rho}_i)$ is the embedding energy of atom i in the host electron density $\bar{\rho}_i$ induced at site i by all other atoms of the system. The host electron density is defined as

$$\bar{\rho}_i = \sum_{j \neq i} \rho_{s_j}(r_{ij}), \quad (2)$$

where $\rho_{s_j}(r_{ij})$ is the electron density function assigned to atom j. The first two terms in Eq. (1) constitute the functional form of the regular EAM[19,20] and have a central-force character, that is, do not depend on angles between interatomic bonds. The noncentral interactions are represented by the last three terms in Eq. (1), which depend on the dipole vectors,

$$\mu_i^\alpha = \sum_{j \neq i} u_{s_i s_j}(r_{ij}) r_{ij}^\alpha, \quad (3)$$

and the quadrupole tensors,

$$\lambda_i^{\alpha\beta} = \sum_{j \neq i} w_{s_i s_j}(r_{ij}) r_{ij}^\alpha r_{ij}^\beta, \quad (4)$$

ν_i being the trace of $\lambda_i^{\alpha\beta}$,

$$\nu_i = \sum_\alpha \lambda_i^{\alpha\alpha}. \quad (5)$$

Equations (3) and (4) introduce two additional pairwise functions, $u_{s_i s_j}(r)$ and $w_{s_i s_j}(r)$, which represent angular-dependent forces. The angular terms penalize the total energy for deviations of atomic environments from cubic symmetry. They vanish in a perfect cubic structure but can be important in noncubic structures and even in cubic structures under nonhydrostatic strains. They can affect elastic constants, defect

formation energies, the melting point, and a number of other properties of the material.

A complete ADP description of the binary Al-Cu system requires 13 functions: $\Phi_{\text{AlAl}}(r)$, $\Phi_{\text{AlCu}}(r)$, $\Phi_{\text{CuCu}}(r)$, $\rho_{\text{Al}}(r)$, $\rho_{\text{Cu}}(r)$, $F_{\text{Al}}(\bar{\rho})$, $F_{\text{Cu}}(\bar{\rho})$, $u_{\text{AlAl}}(r)$, $u_{\text{AlCu}}(r)$, $u_{\text{CuCu}}(r)$, $w_{\text{AlAl}}(r)$, $w_{\text{AlCu}}(r)$, and $w_{\text{CuCu}}(r)$. In this work we used the existing EAM potentials for Al[21] and Cu[22] and constructed only the cross-interaction functions $\Phi_{\text{AlCu}}(r)$, $u_{\text{AlCu}}(r)$, and $w_{\text{AlCu}}(r)$. Since both Al and Cu potentials are the regular EAM type, we formally added the fictitious functions $u_{\text{AlAl}}(r)$, $w_{\text{AlAl}}(r)$, $u_{\text{CuCu}}(r)$, and $w_{\text{CuCu}}(r)$ set to identical 0. It should be noted that, as with all semiempirical models, the choice of the ADP format over EAM cannot be justified rigorously on the basis of the electronic structure of these two metals or their compounds. We chose the ADP format because we were able to achieve a more accurate fit using this format rather than EAM, apparently due to the greater flexibility of the ADP functions and the additional fitting parameters.

The cross-pair function $\Phi_{\text{AlCu}}(r)$ was represented by a cubic spline through a set of $n = 15$ points $\{r_i, \Phi_i\}$ ($i = 1, \ldots, n$). The last point in the set was $(r_c, 0)$, where r_c is the cutoff radius. On the last segment, $[r_{n-1}, r_n]$, the spline was additionally smoothed to make it vanish at r_c together with the first and second derivatives. The distances $\{r_i\}$ were chosen in advance and were not varied during the fit. Thus, $\Phi_{\text{AlCu}}(r)$ was parameterized by a total of 15 parameters: $\{\Phi_i\}$ ($i = 1, \ldots, 14$), and r_c. The cross-dipole and cross-quadrupole functions were parameterized in the form

$$u_{\text{AlCu}}(r) = \left(d_1 e^{-d_2} + d_3\right) \psi\left(\frac{r - r_c}{h}\right), \quad (6)$$

$$w_{\text{AlCu}}(r) = \left(q_1 e^{-q_2} + q_3\right) \psi\left(\frac{r - r_c}{h}\right). \quad (7)$$

Here, d_i, q_i ($i = 1, 2, 3$), and h are the fitting parameters and $\psi(x)$ is a cutoff function defined by

$$\psi(x) = \begin{cases} x^4/(1 + x^4), & x < 0, \\ 0, & x \geqslant 0. \end{cases} \quad (8)$$

The potential transformation coefficients[6] s_{Cu}, g_{Al}, and g_{Cu} were also used as fitting parameters. Thus, the parametrization of the cross-functions involved the total of 25 parameters.

The fitting database included first-principles values for the lattice parameter a of the θ' phase and the formation energies ΔE_f of the θ and θ' phases computed by Wolverton *et al.*[4] It also included the elastic constants c_{ij} of the θ' phase calculated by Vaithyanathan *et al.*[23] The experimental part of the database included lattice parameters[24] a, c, and x and elastic constants[25] c_{ij} of the θ phase. Additionally, the database included first-principles results[10,11,26] for the formation energies of six ordered structures of the Al-Cu system: one stable phase (AlCu$_3$-D0$_{22}$), two metastable phases (Al$_3$Cu$_2$-D5$_{19}$ and AlCu$_3$-D0$_3$), and three imaginary compounds (AlCu-L1$_0$, AlCu-B$_{32}$, and AlCu$_3$-L1$_2$). The formation energy ΔE_f of a compound Al$_n$Cu$_m$ is defined relative to pure fcc Al and pure fcc Cu as

$$\Delta E_f = \frac{1}{n + m}[E(\text{Al}_n\text{Cu}_m) - nE_{\text{fcc}}(\text{Al}) - mE_{\text{fcc}}(\text{Cu})]. \quad (9)$$
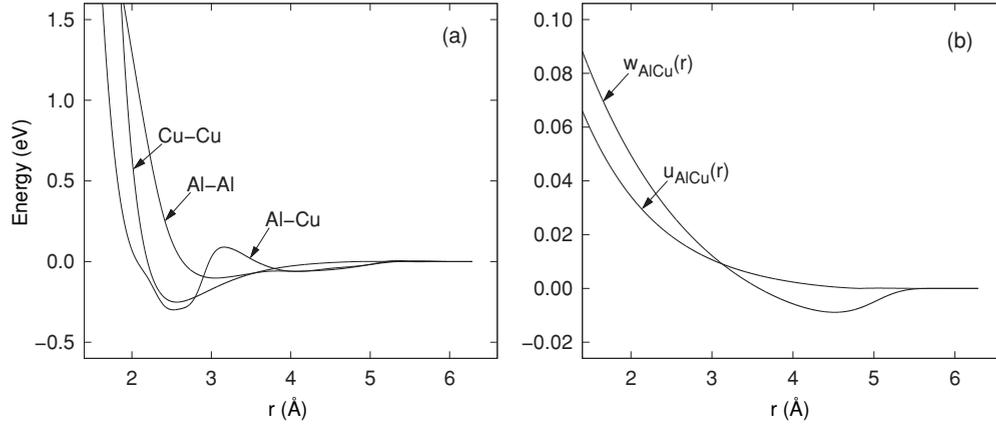
FIG. 1. Potential functions for the Al-Cu system: (a) pair interaction functions; (b) cross-dipole $u_{AlH}(r)$ ($\sqrt{eV}/Å$) and cross-quadrupole $w_{AlH}(r)$ ($\sqrt{eV}/Å^2$) functions.

The cross-functions were optimized by minimizing the weighted mean-squared deviation of the selected properties from their target values using the simulated annealing method.[27] The properties a, ΔE_f, and c_{ij} of the θ' phase were included in the fit with the largest weight. A medium weight was assigned to a, c, x, ΔE_f, and c_{ij} of the θ phase. The formation energies of the Al-Cu compounds were included with the lowest weight. The optimized potential functions are plotted in Fig. 1. The tabulated forms of the functions can be downloaded from the NIST Interatomic Potentials Repository at http://www.ctcms.nist.gov/potentials.

III. TESTING AND VALIDATION OF THE POTENTIAL

Table I summarizes the properties of the θ' phase predicted by the ADP and LLB potentials in comparison with experimental[1] and first-principles[4,23] data. According to experiment,[1] the θ' phase has a slightly distorted C1 structure (CaF$_2$ prototype). For a direct comparison of the lattice parameter a of the undistorted C1 structure calculated from first-principles[4] and with the potentials, the conventional

cell of the experimental bct structure of θ' was rotated by 45° and the experimental lattice parameter a_{exp} was multiplied by $\sqrt{2}$ (Table I). Our potential reproduces a and ΔE_f with very good accuracy. The ADP elastic constants are in reasonable agreement with first-principles results.[23] The LLB potential also gives accurate a and reasonable c_{ij} values. However, it predicts a positive formation energy of the θ' phase instead of a negative one. It should be noted that the θ' phase was in the fit of our potential but not in the LLB fit.

As a test of thermal stability, canonical Monte Carlo (MC) simulations were performed at zero pressure and several temperatures. With the ADP potential, the θ' phase was found to be stable at temperatures up to at least 800 K. By contrast, when computed with the LLB potential, the θ' phase loses stability at $T = 300$ K and transforms to an amorphous structure. We expect that, given enough time, this amorphous structure would eventually crystallize into θ or another crystalline structure, but such long simulations were not pursued in this work. This outcome is not surprising, knowing that the LLB potential predicts a positive ΔE_f of the θ' phase at 0 K.

TABLE I. Properties of the Al$_2$Cu-θ' phase calculated with the ADP (this work) and the LLB[13] potentials in comparison with experimental and first-principles data.

Property	Experiment[a]	*Ab initio*	ADP	LLB
a (Å)	$\sqrt{2}a_{exp} = 5.725$, $c_{exp} = 5.812$	5.68[b]	5.649	5.668
ΔE_f (eV/atom)		−0.199[b]	−0.203	+0.074
Elastic constants (GPa)				
B		117[c]	135.9	199.2
c_{11}		190[c]	192.8	310.5
c_{44}		90[c]	46.5	68.2
c_{12}		80[c]	110.5	142.5
Surface energies (J/m^2)				
$\gamma_s(100)$			1.524	1.093
$\gamma_s(110)$			1.465	1.043
$\gamma_s(111)$			1.768	1.371

[a]From Ref. 1.
[b]From Ref. 4.
[c]From Ref. 23.

TABLE II. Properties of Al_2Cu-θ' computed with the ADP (this work) and the LLB[13] potentials in comparison with experimental and first-principles data.

Property	Experiment	*Ab initio*	ADP	LLB
a (Å)	6.064,[a] 6.067[b]	5.96,[e] 6.067,[f] 6.049[g]	5.935	5.996
c (Å)	4.874,[a] 4.877[b]	4.77,[e] 4.877,[f] 4.891[g]	4.908	4.914
x	0.1586,[a] 0.1581[b]	0.160,[e] 0.1593[g]	0.1671	0.1626
ΔE_f (eV/atom)	-0.135,[c] -0.139 ± 0.031[c]	-0.184,[e] -0.169,[f] -0.170[g]	-0.190	-0.159
Elastic constants (GPa)				
B	113.4[d]	99.4[f]	147.6	137.7
c_{11}	186.2[d]	150.3[f]	199.3	200.3
c_{33}	179.4[d]	171.7[f]	278.2	235.6
c_{44}	29.2[g]	29.4[f]	78.6	59.7
c_{66}	47.2[d]	45.5[f]	21.2	39.8
c_{12}	71.5[d]	86.1[f]	98.2	94.4
c_{13}	79.2[d]	62.6[f]	116.0	98.7
Surface energies (J/m^2)				
$\gamma_s(100)$			1.294	1.266
$\gamma_s(110)$			1.463	1.522

[a]From Ref. 24.
[b]From Ref. 28.
[c]From Ref. 1.
[d]From Ref. 25.
[e]From Ref. 4.
[f]From Ref. 10.
[g]From Ref. 26.

Fully relaxed low-index surface energies γ_s of the θ' phase at 0 K are reported in Table I. We are not aware of experimental or first-principles data that could be used for comparison. Both potentials predict that $\gamma_s(110) < \gamma_s(100) < \gamma_s(111)$ but the ADP energies are consistently higher. This is in agreement with the observation[6] that EAM potentials tend to underestimate surface energies of metals and intermetallic compounds. MC simulations with the ADP potential show that the θ' surfaces remain stable up to at least 800 K. With the LLB potential, the presence of the (111) surface causes instability and amorphization of the θ' phase already at 100 K. We can conclude that the LLB potential cannot be used for atomistic simulations of the θ' phase at finite temperatures.

Properties of the θ phase calculated with the potentials are compared with experimental data[1,24,25,28] and first-principles calculations[4,10,26] in Table II. Both potentials reproduce accurate lattice parameters and the formation energy of this phase. The elastic constants are also in reasonable agreement with the target values. For the relaxed energies of the (100) and (110) surfaces, both potentials give close results but they cannot be compared with first-principles or experimental data. MC simulations with both potentials show that the θ phase, with or without surfaces, remains stable at temperatures up to at least 800 K.

To evaluate the relative stability of the θ and θ' phases at finite temperatures, their Gibbs free energies G per atom were computed with the ADP potential. We used supercells of $N = 768$ atoms with periodic boundary conditions in all directions. At zero pressure

$$G(V,T) = E(V,T) + G^{\text{vib}}(V,T). \quad (10)$$

Here, V is the atomic volume and $E(V,T)$ is the potential energy due to static interactions between atoms, which depends on the temperature due to the temperature dependence of the equilibrium lattice constant. $G^{\text{vib}}(V,T)$ is the contribution from atomic vibrations, which can be computed from the harmonic expression

$$G^{\text{vib}}(V,T) = \frac{k_B T}{N} \sum_{\alpha=1}^{3N-3} \ln \left[2 \sinh \left(\frac{h\nu_\alpha}{2k_B T} \right) \right]. \quad (11)$$

Here h and k_B are Planck's and Boltzmann's constants and ν_α are frequencies of normal vibrational modes of the supercell. Equation (11) is the general quantum-mechanical expression. In the classical limit (all $h\nu_\alpha \ll k_B T$) it becomes

$$G^{\text{vib}}_{\text{classical}}(V,T) = \frac{k_B T}{N} \sum_{\alpha=1}^{3N-3} \ln \left(\frac{h\nu_\alpha}{k_B T} \right). \quad (12)$$

We used the quasiharmonic (QH) approximation,[29] which includes thermal expansion and treats ν_α as volume-dependent quantities. At each temperature, $G(V,T)$ is minimized with respect to the atomic volume to determine the equilibrium lattice constant. The free energies of the θ and θ' phases per atom are plotted as functions of temperature in Fig. 2. This plot shows that at low temperatures, the θ' phase is more stable than θ, in agreement with first-principles calculations.[4] The curves cross and the stability reverses at $T = 325$ K if the quantum-mechanical expression for G^{vib} [Eq. (11)] is used and at $T = 370$ K if the classical expression $G^{\text{vib}}_{\text{classical}}$ [Eq. (12)] is used. In this temperature range, there is a slight difference between the calculated G^{vib} and $G^{\text{vib}}_{\text{classical}}$. Because the quantum-mechanical treatment is physically more
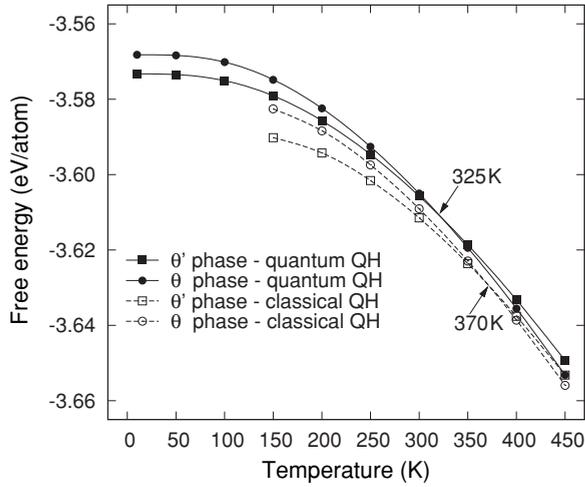
FIG. 2. Free energies per atom of the θ' and θ phases versus temperature calculated with the ADP potential within the quasiharmonic (QH) approximation. Filled squares and circles denote the quantum-mechanical QH results for the θ' and θ phases, respectively. Open squares and circles denote the classical QH results for the θ' and θ phases, respectively. Solid and dashed lines interpolate between the calculated points. The θ' and θ phases reverse their stability at $T = 325$ K for the quantum QH calculations and at $T = 370$ K for the classical QH calculations.

accurate, the predicted phase transformation temperature is 325 K. However, for classical molecular dynamics simulations the observed transformation temperature is predicted to be 370 K.

Both temperatures of the $\theta' \rightarrow \theta$ transformation are somewhat closer to the experimental value[30] of 463 K and the first-principles value[4] of 473 K than the temperature of 260 K obtained with the MEAM potential.[14] In addition, the ADP potential gives the transformation entropy of 0.336 k_B/atom (quantum QH calculations) and 0.395 k_B/atom (classical QH calculations), in good agreement with the first-principles result[4] of 0.37 k_B/atom.

The formation energies of selected Al-Cu compounds calculated with the potentials and from first-principles[4,10,11,26] are listed in Table III. The ADP potential overestimates the energies of most of the Al-Cu compounds tested. The LLB potential underestimates the energy of the metastable phase Al$_3$Cu$_2$-D5$_{19}$ but predicts a better phase stability for 50:50 and Cu-rich compositions. Although neither of the two potentials reproduces the entire convex hull of the 0 K formation energies in full agreement with first-principles data, the general stability trends are reasonable. During the ADP potential fit we sacrificed some of the accuracy of global phase stability to focus on the θ and θ' phases.

Table IV reports fully relaxed dilute heats of solution ΔE_s and solute-vacancy binding energies ΔE_b for Cu in Al and Al in Cu calculated with the potentials. For comparison, experimental[9,31–33] and first-principles[34,35] data are included. For two fcc metals, A and B, the dilute heat of solution of B in A is defined as

$$\Delta E_s = E(A_{n-1}B) - [(n - 1)E_{\text{fcc}}(A) + E_{\text{fcc}}(B)], \quad (13)$$

where n is the total number of atoms in the cell. The calculations were performed for a set of n values, followed by

TABLE III. Formation energies, ΔE_f (eV/atom), of selected Al-Cu compounds predicted by the present ADP potential and the LLB potential[13] in comparison with first-principles data when available. Energy values marked followed by an asterisk were included in the ADP potential fit. Values in boldface are in better agreement with first-principles data.

Formula	Structure	ΔE_f (eV/atom)		
		Ab initio	ADP	LLB
Al$_3$Cu	L1$_2$		0.100	−0.120
Al$_2$Cu-θ'	C1	−0.199[a]	**−0.203***	0.074
Al$_2$Cu-θ	C16	−0.184[a]	**−0.190***	−0.159
Al$_3$Cu$_2$	D5$_{19}$	−0.164,[b] −0.173[c]	−0.345	−0.047
AlCu	B$_2$	−0.195[d]	−0.635	**−0.171**
AlCu	"40" (NbP)	−0.191[d]	−0.257	**−0.181**
AlCu	L1$_0$	−0.147[d]	**−0.076***	−0.253
AlCu	L1$_1$	−0.086[d]	0.090	**−0.145**
AlCu	B8$_1$	−0.043[c]	**−0.170**	0.080
AlCu	B$_{32}$	0.024[d]	−0.085*	**0.021**
AlCu	B$_1$		−0.079	0.195
Al$_4$Cu$_9$	D8$_3$	−0.215[c]	−0.331	**−0.147**
AlCu$_3$	D0$_{22}$	−0.185[c]	−0.245*	**−0.195**
AlCu$_3$	L1$_2$	−0.182[b]	**−0.162***	−0.237
AlCu$_3$	D0$_3$	−0.169[c]	−0.272*	**−0.107**
AlCu$_3$	D0$_{23}$		−0.209	−0.215

[a]From Ref. 4.
[b]From Ref. 10.
[c]From Ref. 26.
[d]From Ref. 11.

linear extrapolation to $1/n \rightarrow 0$.[36] The first-principles result was obtained for $n = 64$.[34]

To evaluate ΔE_b, we first computed the formation energy of a solute-vacancy pair ΔE_f.

$$\Delta E_f = E(A_{n-2}B_1 + V) - [(n - 2)E_{\text{fcc}}(A) + E_{\text{fcc}}(B)], \quad (14)$$

for several n and extrapolated to $1/n \rightarrow 0$. ΔE_b was then calculated from the equation

$$\Delta E_b = -\Delta E_f + \Delta E_s + \Delta E_v, \quad (15)$$

TABLE IV. Dilute heat of solution ΔE_s and solute-vacancy binding energy ΔE_b calculated with the present ADP potential and LLB potential[13] in comparison with experimental and *ab initio* data.

	ΔE_s (eV)		ΔE_b (eV)	
	Cu in Al	Al in Cu	Cu in Al	Al in Cu
Experiment	−0.142[a]	−0.873[b]	0.00 ± 0.12[c]	0.15 ± 0.10[d]
Ab initio	−0.121[e]		0.04[f]	
ADP	−0.181	−0.809	0.075	0.006
LLB	−0.095	−0.836	−0.005	−0.051

[a]From Ref. 9.
[b]From Ref. 31.
[c]From Ref. 32.
[d]From Ref. 33.
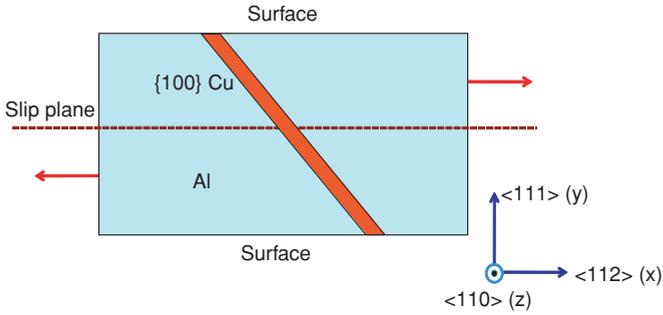[e]From Ref. 34.
[f]From Ref. 35.

FIG. 3. (Color online) Schematic presentation of the supercell used for testing the unrelaxed GP zones for shear.

where ΔE_v is the vacancy formation energy in pure A. The values of ΔE_v are 0.675 eV for pure Al[21] and 1.272 eV for pure Cu.[22] A positive binding energy indicates attractive interaction, consistent with the convention in the literature. Both the ADP and the LLB potentials reproduce the experimental[32,33] and first-principles[35] results for ΔE_b with a reasonable accuracy, especially considering that the magnitude of this quantity is small. Both potentials predict that ΔE_s of Cu in Al is significantly smaller in magnitude than ΔE_s of Al in Cu, which is in good agreement with experiment.[9,31] It should be noted that the LLB potential was fitted to the dilute heats of solution, while the ADP potential was not.

IV. UNIFORM SHEARING OF GP ZONES

As a further test, we computed the energy as a function of displacement during the shearing of an unrelaxed GP zone using the ADP and LLB potentials and first-principles calculations. The simulation block (Fig. 3) contained six (111) Al layers with a total of 96 atoms. The lattice parameter had the equilibrium value calculated with the potentials and by first-principles methods, respectively. By doubling the period of the block in the $\langle 111 \rangle$ direction, two free surfaces were created. The block had periodic boundary conditions in the $\langle 110 \rangle$ and $\langle 112 \rangle$ directions parallel to the (111) plane. One of

the eight (200) Al layers contained in the block was replaced by Cu atoms, creating a structure similar to a GP zone.

To produce shearing, one half of the block above a (111) plane was shifted rigidly in small steps with respect to the other half in either [110] or [$1\bar{1}2$] crystallographic directions. After each step, the generalized stacking fault (GSF) energy, γ_{GSF}, was computed as the excess energy per unit area:

$$\gamma_{\text{GSF}} = \frac{E(x) - E(0)}{S}. \qquad (16)$$

Here $E(x)$ is the total energy of the block for a displacement x in the slip direction and S is the cross-sectional area of the block. For comparison, the GSF energy in pure Al was computed by implementing the same procedure but without the Cu layer. A comparison between the two calculations permits evaluation of the effect of the Cu layer on the shear resistance.

It should be emphasized that no atomic relaxation was performed after the introduction of the Cu layer or during the shearing. Under real conditions, the large atomic size mismatch between Al and Cu produces an elastic strain field around a GP zone. This field strongly affects the dislocation motion and contributes to the strengthening effect. Furthermore, in reality the shearing occurs by the passage of discrete dislocations, not as a uniform translation of half-crystals as in our calculation. Thus, although the geometry of our system is reminiscent of GP zones, this test should not be considered as modeling of the actual GP zone shearing process. The latter would require a much larger system, which cannot be afforded by first-principles methods. Instead, our goal was to perform a severe test of the potentials against first-principles calculations by creating relevant but highly nonequilibrium configurations that were not in the fitting database.

The first-principles density functional theory calculations used the projector augmented wave (PAW) method[37,38] and the Perdew-Wang generalized gradient approximation[39] (GGA-PW91) as implemented in the Vienna *ab initio* simulation package (VASP).[40,41] We used the Methfessel-Paxton smearing method[42] with a smearing width of 0.2 eV and a large cutoff energy of 380 eV in all calculations. An $(18 \times 18 \times 18)$ Monkhorst-Pack[43] k-point mesh sampling the Brillouin zone
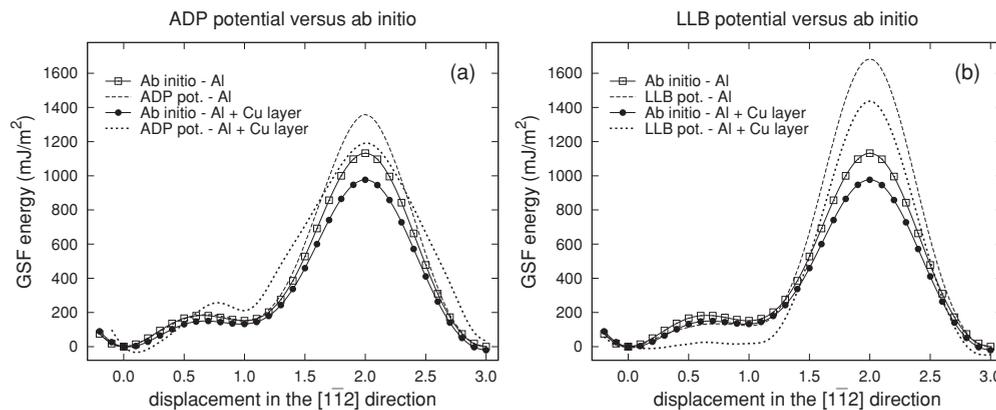

FIG. 4. Unrelaxed GSF energy versus displacement for shear along the [$1\bar{1}2$] direction for pure Al and Al with a (100) Cu layer: (a) calculated with the ADP potential and (b) calculated with the LLB potential.[13] *Ab initio* data computed in this work are included for comparison. Displacement is measured in units of the partial Burgers vector $(1/6)[1\bar{1}2]$. Solid curves interpolate between the *ab initio* data points.
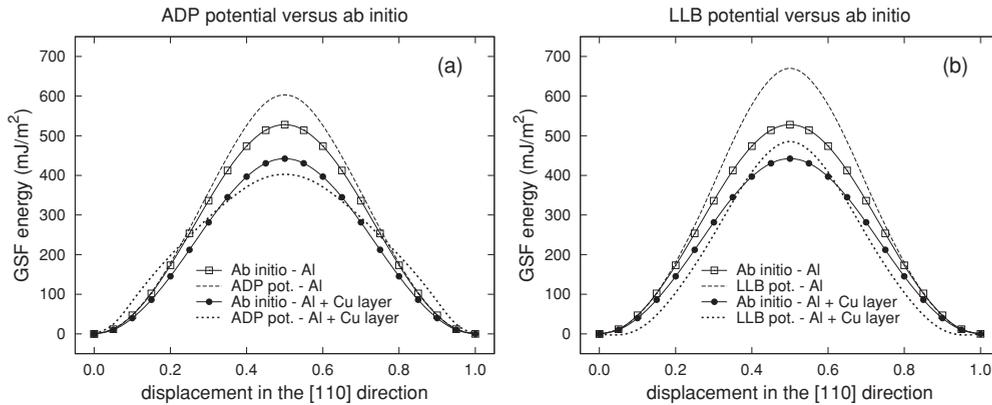
FIG. 5. Unrelaxed GSF energy versus displacement for shear along the [110] direction for pure Al and Al with a (100) Cu layer: (a) calculated with the ADP potential and (b) calculated with the LLB potential.[13] *Ab initio* data computed in this work are included for comparison. Displacement is measured in the units of the perfect Burgers vector (1/2)[110]. Solid curves interpolate between the *ab initio* data points.

of the primitive unit cell of bulk fcc Al was rescaled to a $(4 \times 12 \times 1)$ grid appropriate for the slab geometry. This ensured the energy convergence to within 1 meV/atom. As a test, the energy-volume curve for fcc Al was computed and fitted by the Birch-Murnagham's equation of state.[44] The obtained equilibrium lattice parameter and the bulk modulus of Al, 4.047 Å and 74.50 GPa, are in excellent agreement with the experimental values[45] of 4.05 Å and 77.3 GPa, respectively.

As an additional check, the relaxed intrinsic stacking fault energy in pure Al was computed using the same block and optimizing the atomic positions by a conjugate-gradient algorithm. The convergence criterion for Hellman-Feynman forces on each atom was set to 5 meV/Å. The relaxed stacking fault energy was found to be 146.5 mJ/m^2 in good agreement with other first-principles results reported in the literature: 143 mJ/m^2,[46] 164 mJ/m^2,[47] and 134 mJ/m^2 (calculated with VASP).[48]

Figures 4 and 5 show the GSF energy curves for the [1$\bar{1}$2] and [110] directions, respectively, with and without the Cu layer. The first and obvious conclusion is that neither of the two potentials matches the first-principles calculations accurately. However, the ADP potential appears to be in better agreement with the VASP results. The LLB potential overestimates the height of the large peak more significantly than the ADP potential does. In addition, the LLB potential predicts an unrealistically large softening of the material for shear in the [1$\bar{1}$2] direction in the presence of the Cu layer. The VASP calculation gives only a small reduction in energy due to the Cu layer. The ADP potential predicts a decrease and then an increase in energy but, on average, follows the trend computed with VASP. The unrelaxed GSF energies for the displacement by one partial Burgers vector (1/6)[1$\bar{1}$2] in the presence of Cu are 132.4 mJ/m^2 (VASP), 210.5 mJ/m^2 (ADP), and only 18.2 mJ/m^2 (LLB). The latter number indicates that, with the LLB potential, the system would virtually lose resistance to sliding due to the introduction of the Cu layer.

V. CONCLUSIONS

We have developed an interatomic potential for the Al-Cu system based on the ADP formalism. The potential

incorporates existing elemental EAM potentials for Al[21] and Cu.[22] Only the cross-interaction functions were fitted in this work, using a database of experimental and first-principles data.

The ADP potential reproduces the lattice parameters, formation energies, and elastic properties of the θ and θ' phases of the Al-Cu system, which are relevant to the precipitation hardening of Al-Cu alloys. The potential predicts that the θ' phase is more stable than the θ phase at 0 K and that the vibrational entropy stabilizes θ over θ' at high temperatures. This effect was previously found by first-principles calculations.[4] Using the quasiharmonic approximation, we computed the phase transformation temperature to be 325 K (370 K in the classical approximation). This prediction is in reasonable agreement with first-principles calculations, which give the transformation temperature of 473 K.[4] The entropy of the transformation predicted by the potential is in excellent agreement with first-principles results.[4] Overall, the ADP potential accurately and reliably reproduces the phase stability and the θ-θ' phase transformation in the Al-Cu system.

The ADP potential also reproduces the dilute heats of solution, the vacancy-impurity binding, the stability of alternate compounds of the Al-Cu system, and a number of other properties. As a severe test, the potential was used to compute GSF energies when shearing an unrelaxed structure reminiscent of a GP zone. The results were compared with first-principles calculations of the shearing process performed in this work. The ADP potential does not agree with the first-principles results accurately but captures the essential trends. We note that neither GSF energies nor any related properties were included in the potential fit.

For comparison, all tests of the ADP potential were repeated with the previously developed EAM potential referred to as the LLB.[13] The latter gives more accurate results for some of the properties tested but less accurate results for others. A significant disadvantage of the LLB potential is that it gives the wrong sign of the formation energy of the θ' phase. In fact, the latter loses thermodynamic stability at finite temperatures, preventing the LLB potential from being useful for atomistic simulations of the θ' precipitation in

Al-Cu alloys. The LLB potential is also in poorer agreement with the first-principles results for the GP-zone shearing. We conclude that the ADP potential developed in this work demonstrates improvements over previous semiempirical potentials for the Al-Cu system and could be used in atomistic simulations of precipitation hardening in Al-Cu alloys. This potential was recently employed in molecular dynamics simulations of the effect GP zones on dislocation motion in Al.[5]

*fapostol@gmu.edu

†Corresponding author: ymishin@gmu.edu

[1] J. L. Murray, Int. Metals Rev. **30**, 211 (1985).

[2] A. Guinier, Nature **142**, 569 (1938).

[3] G. D. Preston, Proc. R. Soc. London A **167**, 526 (1938).

[4] C. Wolverton and V. Ozoliņš, Phys. Rev. Lett. **86**, 5518 (2001).

[5] C. V. Singh and D. H. Warner, Acta Mater. **58**, 5797 (2010).

[6] Y. Mishin, *Handbook of Materials Modeling*, edited by S. Yip (Springer, Dordrecht, The Netherlands, 2005), pp. 459–478.

[7] J. Cai and Y. Y. Ye, Phys. Rev. B **54**, 8398 (1996).

[8] R. A. Johnson, Phys. Rev. B **39**, 12554 (1989).

[9] I. Ansara, A. T. Dinsdale, and M. H. Rand, eds., *COST 507: Thermodynamic Database for Light Metal Alloys*, Vol. 2 (European Commision, Brussels, 1998).

[10] W. Zhou, L. Liu, B. Li, Q. Song, and P. Wu, J. Electron. Mater. **38**, 356 (2009).

[11] D. Nguyen-Manh and D. G. Pettifor, Intermetallics **7**, 1095 (1999).

[12] C. L. Rohrer, Modell. Simul. Mater. Sci. Eng. **2**, 119 (1994).

[13] X. Y. Liu, C. Y. Liu, and L. J. Borucki, Acta Mater. **47**, 3227 (1999).

[14] S. Y. Hu, M. I. Baskes, M. Stan, and L. Q. Chen, Acta Mater. **54**, 4699 (2006).

[15] Y. Mishin, M. J. Mehl, and D. A. Papaconstantopoulos, Acta Mater. **53**, 4029 (2005).

[16] Y. Mishin and A. Y. Lozovoi, Acta Mater. **54**, 5013 (2006).

[17] A. Hashibon, A. Y. Lozovoi, Y. Mishin, C. Elsässer, and P. Gumbsch, Phys. Rev. B **77**, 094131 (2008).

[18] F. Apostol and Y. Mishin, Phys. Rev. B **82**, 144115 (2010).

[19] M. S. Daw and M. I. Baskes, Phys. Rev. Lett. **50**, 1285 (1983).

[20] M. S. Daw and M. I. Baskes, Phys. Rev. B **29**, 6443 (1984).

[21] Y. Mishin, D. Farkas, M. J. Mehl, and D. A. Papaconstantopoulos, Phys. Rev. B **59**, 3393 (1999).

[22] Y. Mishin, M. J. Mehl, D. A. Papaconstantopoulos, A. F. Voter, and J. D. Kress, Phys. Rev. B **63**, 224106 (2001).

[23] V. Vaithyanathan, C. Wolverton, and L. Q. Chen, Phys. Rev. Lett. **88**, 125503 (2002).

[24] Y. Grin, F. R. Wagner, M. Armbrüster, M. Kohout, A. Leithe-Jasper, U. Schwarz, U. Wedig, and H. G. von Schnering, J. Solid State Chem. **179**, 1707 (2006).

[25] F. R. Eshelman and J. F. Smith, J. Appl. Phys. **49**, 3284 (1978).

[26] Alloy database, [http://alloy.phys.cmu.edu/] (2005).

[27] S. Kirkpatrick, C. D. Gelatt, and M. P. Vecchi, Science **220**, 671 (1983).

[28] A. Meetsma, J. L. de Boer, and S. van Smaalen, J. Solid State Chem. **83**, 370 (1989).

[29] S. M. Foiles, Phys. Rev. B **49**, 14930 (1994).

[30] J. M. Silcock, T. J. Heal, and H. K. Hardy, J. Inst. Met. **82**, 239 (1953).

[31] J. L. Murray, cited in Ref. 12 (as "private communication, 1992").

[32] A. D. King and J. Burke, Acta Metall. **18**, 205 (1970).

[33] M. Doyama, K. Kuribayashi, S. Nanao, and S. Tanigawa, Cryst. Lattice Defects **4**, 255 (1973).

[34] C. Ravi, C. Wolverton, and V. Ozoliņš, Europhys. Lett. **73**, 719 (2006).

[35] C. Wolverton, Acta Mater. **55**, 5867 (2007).

[36] Y. Mishin, M. R. Sørensen, and A. F. Voter, Philos. Mag. A **81**, 2591 (2001).

[37] P. E. Blochl, Phys. Rev. B **50**, 17953 (1994).

[38] G. Kresse and D. Joubert, Phys. Rev. B **59**, 1758 (1999).

[39] J. P. Perdew, J. A. Chevary, S. H. Vosko, K. A. Jackson, M. R. Pederson, D. J. Singh, and C. Fiolhais, Phys. Rev. B **46**, 6671 (1992).

[40] G. Kresse and J. Furthmüller, Comput. Mater. Sci. **6**, 15 (1996).

[41] G. Kresse and J. Furthmüller, Phys. Rev. B **54**, 11169 (1996).

[42] M. Methfessel and A. T. Paxton, Phys. Rev. B **40**, 3616 (1989).

[43] H. Monkhorst and J. Pack, Phys. Rev. B **13**, 5188 (1976).

[44] F. Birch, Phys. Rev. **71**, 809 (1947).

[45] W. F. Gale and T. C. Totemeir, eds., *Smithells Metals Reference Book*, 8th ed. (Elsevier Butterworth-Heinemann, London, 2004).

[46] J. Hartford, B. von Sydow, G. Wahnström, and B. I. Lundqvist, Phys. Rev. B **58**, 2487 (1998).

[47] G. Lu, N. Kioussis, V. V. Bulatov, and E. Kaxiras, Phys. Rev. B **62**, 3099 (2000).

[48] G. Lu, D. Orlikowski, I. Park, O. Politano, and E. Kaxiras, Phys. Rev. B **65**, 064102 (2002).